Research Article Open Access

Guobin Xu, Yuejun Zhu, Xiujun Wang, Shanshan Wang, Tianxiang Cheng, Rang Ping, Jie Cao* and Kaihe Lv*

Novel chitosan and Laponite based nanocomposite for fast removal of Cd(II), methylene blue and Congo red from aqueous solution

https://doi.org/10.1515/epoly-2019-0025
Received September 21, 2018; accepted December 11, 2018.

Abstract: A series of chitosan and Laponite based nanocomposite adsorbents, which showed an excellent performance for fast and efficient removal of Cd(II), methylene blue (MB) and Congo red (CR) from aqueous solution, were prepared. In the adsorbent, with the increase of Laponite component, the surface area increased from 44.69 m^2 g^{-1} to 64.58 m^2 g^{-1}. As a result, the adsorption rates were enhanced by increasing Laponite component. The adsorption capacities for Cd(II) and MB increased with increasing Laponite component due the cationic characteristic of two pollutants, and the opposite result was found for the removal of CR. The impacts of some factors, e.g. solution pH, temperature, pollutant concentration and salt, on the adsorption capacity were investigated. Additionally, this adsorbent could be effectively regenerated by dilute HCl solution after the adsorption of Cd(II), and the mixture of methanol and acetic acid was a suitable eluent after the adsorption of two dyes.

Keywords: wastewater treatment; fast adsorption; inorganic-organic hybrid; Laponite; nanocomposite

*** Corresponding authors: Jie Cao and Kaihe Lv,** Shandong Key Laboratory of Oilfield Chemistry, School of Petroleum Engineering, China University of Petroleum (East China), Qingdao 266580, China, e-mail: jcao@upc.edu.cn (Jie Cao); lkh54321@126.com (Kaihe Lv). Tel.: +86 532 86981190, Fax: +86 532 86981936.
Guobin Xu and Rang Ping, College of Chemical Engineering, China University of Petroleum (East China), Qingdao 266580, China.
Yuejun Zhu, Xiujun Wang and Shanshan Wang, State Key Lab of Offshore Oil Exploitation, Beijing 100028, China; CNOOC Research Institute Co. Ltd, Beijing 100028, China.
Tianxiang Cheng, Shandong Key Laboratory of Oilfield Chemistry, School of Petroleum Engineering, China University of Petroleum (East China), Qingdao 266580, China.

1 Introduction

As a result of rapid urbanization and industrialization, water pollution, which is caused by the continuous release of toxic pollutants from heavy metals, dyes, synthetic manure and organic compounds into the encompassed water bodies, has attracted worldwide attention (1-3). Cd(II) is considered as one of the most toxic heavy metal ions. Even at very low concentration, the presence of Cd(II) is tremendously harmful to the water environment and human health in terms of renal disturbances, muscular cramps, high blood pressure, lung insufficiency, proteinuria, bone lesions, destruction of red blood cells and testicular tissues (4). Pollution by Cd(II) usually comes from several industries such as electroplating, metal production, alloy manufacturing, plastic, the combustion of fossil fuels, the manufacturing of batteries, pigments, and screens (5,6). Around 100,000 types of dyes are produced with a yearly production rate of over 7×10^5 to 1×10^6 tons and utilized as a part of a few businesses, for example, material, textile, leather, paper, printing, paint, pigments, rubber and plastic (7). Methylene blue (MB), a cationic dye, is widely used for colouring paper, printing cotton, dyeing leather, and indicating oxidation-reduction in analytical chemistry and also used as an antiseptic (8). Congo red (CR), an anionic dye, is used for dyeing plastic and textile and also used as a biological stain (9). From short time and prolonged contact with MB and CR dyes, many diseases can be caused, such as tissue necrosis, cyanosis, and heart beat increase in humans and also threats to marine life (10).

From wastewater treatment, heavy metal ions and dyes have been removed by various technologies, such as chemical precipitation, ultrafiltration, ion exchange, oxidation/reduction, membrane separation and electrochemical technologies (11-13). However, each method has its inherent limitations, such as high energy consumption, generation of toxic sludge, incomplete

treatment, and high reagent requirement (14). The adsorption method has been developed as a suitable process for the treatment of heavy metal ions from contaminated water or soil because of its low cost, great removal efficiency and simple regeneration (15). For preparing effective adsorbent, efficient adsorption group is crucial for adsorbent. The introduction of different adsorption groups into adsorbent is one of the basic methods to improve the adsorption performance of adsorbent. A lot of adsorbents with novel molecular structures and excellent properties have been prepared and studied (16-18). Additionally, surface area and microstructure are also important for fast adsorption and high removal efficiency (19). High surface area and large amount of micropores in adsorbent is convenient for the penetration of water and heavy metal ions into the interior and thus enhances the adsorption rate and removal efficiency. Additionally, the surface area and microstructure of adsorbent could also affect the utilization of functional groups for adsorption (20,21).

Laponite could be exfoliated into individual particles with a thickness of about 1 nm, and a diameter of about 25 nm in aqueous solution (3). Due to its significant surface area and charged surface, Laponite is suitable for the adsorption of several chemicals (22,23). However, Laponite dispersion cannot be directly mixed with many chemicals to prepare Laponite based nanocomposite because Laponite particles flocculate in salt or polymer solution. It has been reported that nanometer Laponite particles exhibit much better dispersion performance of salt resistance after being pre-adsorbed by 2-acrylamido-2-methylpropanesulfonic acid (AMPS) (24). Chitosan is the most abundant biopolymer after cellulose. Chitosan is regarded as an efficient component in the adsorption of pollutants due to its high content of -NH_2 groups and -OH groups, which are conducive to chelating and surface contact with pollutant molecules (17,25). Up to now, chitosan based materials have been prepared and applied in the removal of Cd(II), Pb(II), Cu(II), Hg(II), Congo red, methylene blue, methyl orange, malachite green and tartrazine from aqueous solution (26).

In our previous experiment, we prepared a novel chitosan and Laponite based hybrid nanocomposite adsorbent (3). The introduction of AMPS into the nanocomposite could obviously improve the dispersion stability of Laponite, which increased the surface area and total pore volume of this adsorbent. As a result, this adsorbent exhibited an excellent adsorption capacity and high adsorption rate for Cu(II). To further understand this kind of adsorbent, the removal of Cd(II), MB and CR from aqueous solution was studied in detail in this paper.

2 Experimental

2.1 Materials

Chitosan with a deacetylation degree of 85% was purchased from Jinan Haidebei Marine Bioengineering Co. (China), and purified twice as follows: it was dissolved in HCl solution with a concentration of 0.1 mol L^{-1}, then the solution was filtered and precipitated with ethanol, and the product was dried in vacuo at 50°C for 48 h. The average molecular weight of chitosan was measured by intrinsic-viscosity method and the result was 2.4×10^5 g mol^{-1}. Laponite XLG ($Mg_{5.34}Li_{0.66}Si_8O_{20}(OH)_4Na_{0.66}$) was obtained from Rockwood (Wesel, Germany). Monomers, including acrylic acid (AA, 98%), acrylamide (AM, 98%), 2-acrylamido-2-methylpropanesulfonic acid (AMPS, 98%), initiator potassium persulfate (KPS, 99%) and crosslinker N,N'-methylenebisacrylamide (MBA, 98%) were obtained from Shanghai Sinopharm Chemical Reagent Co. Ltd. (China). Other chemicals were of analytical grade and used as received.

2.2 Adsorbent preparation

An AA aqueous solution with a concentration of 2 wt% was prepared, and chitosan with a concentration of 5 wt% was dissolved in the solution under agitation for 48 h at room temperature. A transparent Laponite XLG aqueous dispersion was obtained under ultrasonication for 30 min, and the concentration of Laponite was 2 wt%. AMPS was added into the dispersion, and after stirring for 2 h, other chemicals including AM, AA, MBA, and chitosan were added. After stirring for 30 min under a nitrogen atmosphere, 10 g of KPS solution (0.5 wt%) was added and polymerization was performed at 70°C for 4 h. The product was dried under vacuum at 65°C for 48 h and sieved to give 40-20 mesh particles.

2.3 Characterization

The molecular structure of adsorbent was confirmed by Fourier transform infrared spectroscopy (FTIR) on a Tensor 27 spectrometer (Bruker, Switzerland). The sample was prepared as KBr pellet and the result was obtained at a resolution of 4 cm^{-1} in the frequency range of 4000-400 cm^{-1} for a total of 16 scans. Thermogravimetric analysis (TGA) of the adsorbent was performed using a thermogravimetric analyzer (Mettler TGA / SDTA851) under a nitrogen atmosphere at a heating rate

of 10°C min^{-1}. N_2 adsorption-desorption experiment was performed by a specific surface area and pore analyzer (NOVA 3200e, Quantachrome), and the specific surface area, average pore size, and pore size distribution of adsorbent was obtained. Before the experiment, each sample was treated with organic solvents to remove moisture. The specific surface area was calculated according to Brunauer-Emmett-Teller (BET) equation. The volume of adsorbed N_2 at a relative pressure of 0.99 was used to calculate the total pore volume. The desorption isotherm was used to study the pore size distribution via the Barrett-Joyner-Halenda (BJH) method. The average pore size D (nm) was calculated by Eq. 1 (27):

$$D = 4V_{total}/A_{BET} \quad (1)$$

where V_{total} (cm^3 g^{-1}) is the total pore volume, and A_{BET} (m^2 g^{-1}) is the specific surface area.

2.4 Adsorption experiments

The effects of adsorption time, initial solution pH, temperature, salt concentration and equilibrium pollutant concentration on the adsorption capacity of different adsorbents were analyzed by batch adsorption experiments. For each experiment, 0.050 g of adsorbent was added into 50 mL of pollutant solution. The solution was stirred by a magnetic stirrer through the whole adsorption process. After adsorption, the solution was analyzed using an atomic absorption spectrophotometer (Varian Spectra HP 3510) to determine the residual Cd(II) concentration, whereas the equilibrium concentration of dyes was determined with a UV-1780 (Shimadzu, Japan) spectrophotometer. The adsorption capacity q was calculated by Eq. 2:

$$q = \frac{(c_0 - c_e) \times v}{m} \quad (2)$$

where C_0 (mmol L^{-1}) is the initial concentration of pollutant, C_e (mmol L^{-1}) is the concentration of pollutant at equilibrium, V (L) is the volume of solution, and m (g) is the mass of adsorbent used.

2.5 Desorption experiments

After the 90-min adsorption of Cd(II) (50 mL, 500 mg L^{-1}) experiment, the adsorbent (0.05 g) was filtered out from solution. The adsorbed pollutant was removed from the adsorbent being washed in HCl solution (50 mL) for 30 min. And then, the adsorbent was used in the same Cd(II) solution again. For the removal of MB and CR, the regeneration of adsorbent was performed in the same process except that 50 mL of methanol/acetic acid (v/v, 9/1) was used as eluent. The reutilization experiment of adsorbent was performed for 5 consecutive times.

2.6 Model to experimental data

For adsorption kinetic analysis, two models were used to evaluate the time required to remove pollutants.

The pseudo-first-order kinetic model, described as:

$$q_t = q_e - q_e e^{-k_1 t} \quad (3)$$

where q_t and q_e are adsorption capacity (mmol g^{-1}) at time t (min) and at equilibrium respectively, k_1 (min^{-1}) is the kinetic rate constant.

The pseudo-second-order kinetic model, defined as:

$$q_t = \frac{k_2 q_e^2 t}{1 + k_2 t q_e} \quad (4)$$

where k_2 (g $mmol^{-1}$ min^{-1}) is the pseudo-second-order rate constant.

For adsorption isotherm analysis, two common isotherm models were employed to fit the experimental data.

The first adsorption isotherm model is the Langmuir isotherm model expressed by Eq. 5:

$$q_e = \frac{k_L q_m c_e}{1 + k_L c_e} \quad (5)$$

where q_e (mg g^{-1}) is the equilibrium adsorption capacity of the adsorbent, C_e is the equilibrium pollutant concentration in solution (mg L^{-1}), q_m (mg g^{-1}) is the maximum adsorption capacity of the adsorbent, and K_L (L mg^{-1}) is the Langmuir adsorption constant.

The second adsorption isotherm model is the Freundlich isotherm model, which is expressed as:

$$q_e = K_F C_e^{1/n} \quad (6)$$

where q_e and C_e are defined as above, K_F (L mg^{-1}) is the Freundlich constant, and n is the heterogeneity factor.

3 Results and discussion

3.1 Characterization of adsorbents

The molecular structures of four samples (Table 1) were analyzed by FTIR analysis, and the results are shown

in Figure 1. The FTIR spectra exhibit O-H stretches near 3551 cm^{-1}, the C-H stretching vibrations around 2932 cm^{-1}, and the C-H bending vibrations around 1450 cm^{-1}. The characteristic peaks around 1034 cm^{-1} and 1184 cm^{-1} are attributed to the absorption band of sulfonic group. The peak at 1109 cm^{-1} is classically assigned to the absorption band of polysaccharide molecule backbone, which indicates the introduction of chitosan component in four samples (3). In general, the broad peak at around 1800-1600 cm^{-1} corresponds to the absorption band of carbonyl group in ketone, carboxylic acid, carboxylate and amide, furthermore, the carbonyl group in carboxylic acid usually exhibits a high absorption peak at around 1750 cm^{-1}. As a result, the peak at 1728 cm^{-1} could be attributed to the absorption of carboxylic acid, and this is consistent with the adsorbent preparation process (acidic condition). The peaks at 519 and 455 cm^{-1} are attributed to the absorption band of Si-O from Laponite component, and the absorption intensity of these peaks continuously increases from S-1 to S-4, which is consistent with the gradual increase of the feeding ratio of Laponite (28).

It has been reported that the incorporation of inorganic nanoparticles into polymer matrix is expected to improve its surface properties, such as its surface area and pore diameter (29). The microstructure difference in the four adsorbents was investigated by BET analysis as shown in Figure 2 and Table 2. For S-4, the BET surface area and pore volume are measured to be 64.58 $m^2\ g^{-1}$ and 0.1713 $cm^3\ g^{-1}$. However, the BET surface area and pore volume for S-1 are only 44.69 $m^2\ g^{-1}$ and 0.0772 $cm^3\ g^{-1}$, which are much smaller than S-4. This reflects that the increase of Laponite component could enhance the surface area and total pore volume of the adsorbent. For adsorbents with similar molecular structures, higher surface area might be more beneficial for rapid and effective adsorption of pollutant from wastewater. The BJH analysis method was further used for BET results to investigate the pore-size distribution for each sample, and the results are shown in Figure 3. By comparing S-1 and S-3, it is found that S-1 has smaller total pore volume and lower porosity than S-3, and obviously, S-1 has narrower pore-size distribution. Furthermore, it is worth noting that the average pore size also gradually increases with the increase of Laponite component. Thus, for this adsorbent, greater surface area, pore volume, and average pore size are pronounced with more Laponite addition.

The results for TGA measurements and differential thermogravimetric analysis (DTGA) for four samples are shown in Figure 4. For any sample, a mass-loss peak could be observed from 200°C to 280°C, which is generally attributed to the thermal decomposition of chitosan

Table 1: The feeding composition of four samples.

Sample	AM (g)	AA (g)	AMPS (g)	MBA (g)	H_2O (g)	Laponite (g)	Chitosan (g)	KPS (g)	Yield (%)
S-1	5.0	2.5	2.5	0.03	90.0	0.5	0.5	0.05	98.6
S-2	5.0	2.5	2.5	0.03	90.0	1.0	0.5	0.05	98.8
S-3	5.0	2.5	2.5	0.03	90.0	1.5	0.5	0.05	98.2
S-4	5.0	2.5	2.5	0.03	90.0	2.0	0.5	0.05	97.9

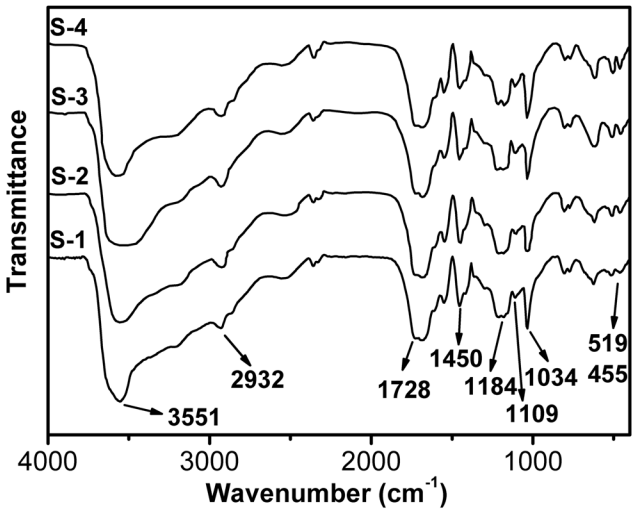

Figure 1: FTIR analysis of four samples.

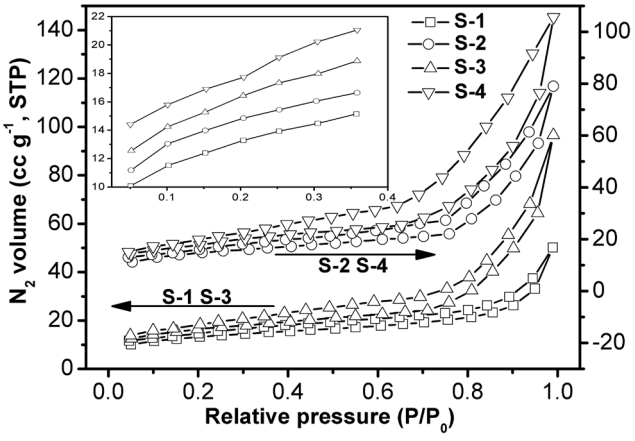

Figure 2: N_2 adsorption-desorption isotherms of four adsorbents (inset, adsorbed N_2 volume at low pressure).

Table 2: Structural characteristics of four samples.

Sample	A_{BET} ($m^2\ g^{-1}$)	V_{total} ($cm^3\ g^{-1}$)	D (nm)
S-1	44.69	0.0772	6.90
S-2	54.45	0.1216	8.93
S-3	61.63	0.1487	9.65
S-4	64.58	0.1713	10.61

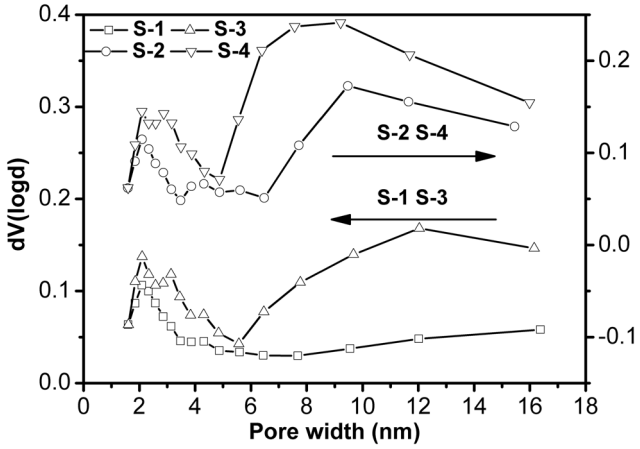

Figure 3: Pore size distributions of four adsorbents.

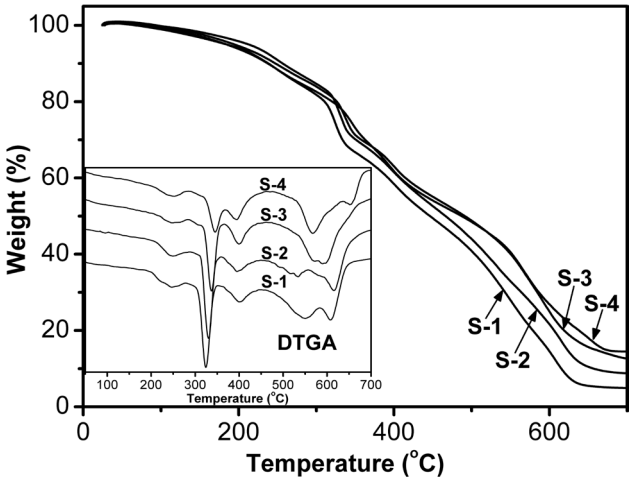

Figure 4: TGA and DTGA curves of four adsorbents.

component and the imidization reaction between amide groups on polymer backbone (30,31). The maximum mass-loss peak during the whole thermal degradation process is found at around 330°C, and it is interpreted as the breakdown of the polymer backbone and the imides formed in the above decomposition region. However, as shown in DTGA inset, from S-1 to S-4, the temperature for this mass-loss process is 324°C, 330°C, 337°C and 345°C, respectively, which could indicate that the thermal stability of polymer backbone is reinforced due to the increase of Laponite. Additionally, the residual weight percentage of thermal decomposition at 700°C is in the same order of Laponite concentration because inorganic component is more stable at high temperature.

3.2 Adsorption studies

3.2.1 Adsorption kinetics

From adsorption kinetics investigation, key information about the adsorption rate and the pathway for adsorption process can be obtained, which could mostly determine the potential applications of adsorbent. The relationship between adsorption capacity and contact time by four samples is illustrated in Figure 5. It can be seen that four adsorbents have rapid adsorption rate compared to conventional polymeric adsorbent. The increase of Laponite component in adsorbent will improve the adsorption rate. For example, for the removal of Cd(II), the adsorption equilibrium time for S-3 and S-4 is 20 min, and that for S-2 and S-1 is 25 min and 35 min, respectively. This can be attributed to the increase of surface area and pore volume by the formation of nanocomposite in the adsorbent.

For the removal of Cd(II), the adsorption capacity happens in the order of S-3 (0.47 mmol g^{-1}) > S-4 (0.43 mmol g^{-1}) > S-2 (0.4 mmol g^{-1}) > S-1 (0.36 mmol g^{-1}). For an adsorbent, the adsorption is induced by the combination interaction from its different functional groups. As a result, an optimal ratio between different groups exists in this process (32). For the removal of MB, four adsorbents exhibit excellent adsorption capacities, and the removal efficiency for each sample is more than 95%. A slight increase of adsorption capacity with the increase of the Laponite concentration is found, and S-4 presents the best adsorption capacity (0.31 mmol g^{-1}). Different from the above two cases, for the removal of CR, the adsorption capacity continuously reduces with the increase of the Laponite concentration. CR is an anionic compound and Laponite is a high negatively charged component. The electrostatic repulsion between them could be an unfavorable factor for the adsorption (10). S-1 shows the best adsorption capacity (0.091 mmol g^{-1}), and its removal efficiency is 63.4%.

The adsorption kinetics curve fittings by the pseudo-first-order kinetic model and the pseudo-second-order kinetic model have been carried out and the corresponding parameters were calculated as shown in Table 3. For each adsorbent, the higher coefficient of determination (R^2) is

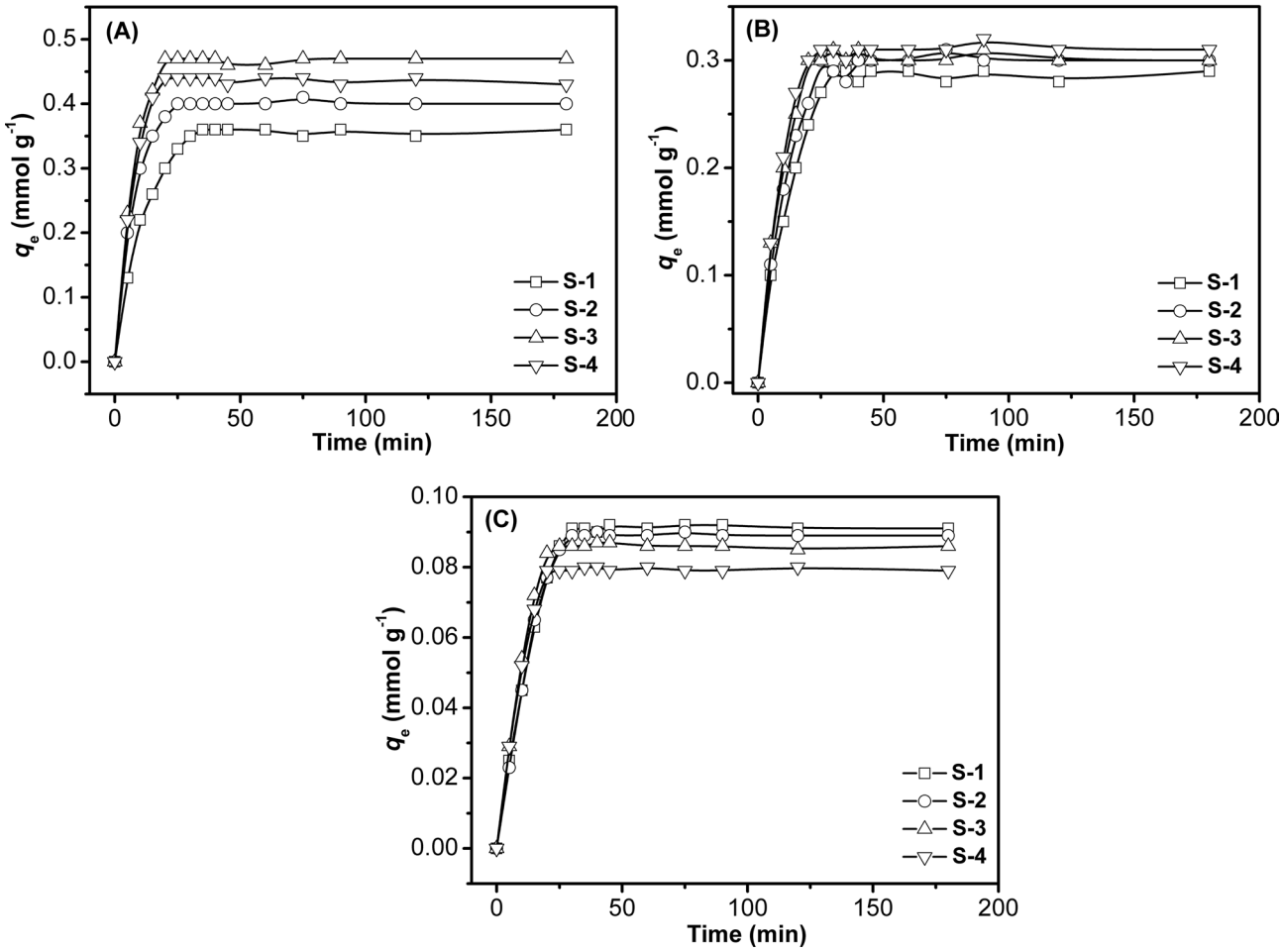

Figure 5: Adsorption kinetic on the adsorption of (a) Cd(II), (b) MB and (c) CR. (Conditions: initial pollutant concentration 100 mg L^{-1}; pH 6.0; 30°C; adsorbent dosage 1 g L^{-1}).

obtained for the pseudo-first-order kinetic model. Moreover, the closer agreement of the calculated equilibrium adsorption capacity (q_e) from the pseudo-first-order kinetics with the experimentally determined value further proves that the adsorption processes for four adsorbents follow the pseudo-first-order kinetic model. Taking the removal of Cd(II) as an example, the numerical result of k_1 (pseudo-first-order model) is in the order of S-4 (0.152) > S-3 (0.148) > S-2 (0.138) > S-1 (0.092). As a result, the increase of Laponite component obviously improves the adsorption rate.

3.2.2 Adsorption isotherm

The amount of adsorbed pollutant versus equilibrium concentrations, which is also called as adsorption isotherm, are shown in Figure 6, and the corresponding parameters from the Langmuir and the Freundlich models are summarized in Table 4. As the pollutant concentration increases, all adsorbent samples have a similar trend in equilibrium adsorption capacity for the removal of Cd(II), MB or CR. For example, for the removal of Cd(II), the adsorption capacity of S-1 increases from 11.0 to 93.7 mg g^{-1} with increasing the initial concentration from 20 to 400 mg L^{-1}, and the adsorption capacity shows a slight increase with further increasing the concentration. With the increase of pollutant concentration, the driving force for the adsorption is enhanced. At lower pollutant concentration, almost all pollutant molecules can contact with the active sites on the surface of adsorbent, as a result, a significant enhancement in the adsorption capacity of adsorbent can be observed with the increase of pollutant concentration. However, the adsorption sites will reach saturation at high pollutant concentration, and a balanced adsorption capacity is found (33).

The Langmuir model assumes that adsorption occurs at specific homogenous sites of adsorbent and all adsorption sites are energetically equivalent (34). However, the Freundlich model is suitable for describing multilayer adsorption on heterogeneous adsorbent surface. The Freundlich model assumes that the distribution of

Table 3: Adsorption kinetics constants for Cd(II), MB and CR adsorbed by four adsorbents.

Sample	Cd(II)						MB						CR					
	Pseudo-first			Pseudo-second			Pseudo-first			Pseudo-second			Pseudo-first			Pseudo-second		
	k_1	q_e	R^2	k_2	q_e	R^2	k_1	q_e	R^2	k_2	q_e	R^2	k_1	q_e	R^2	k_2	q_e	R^2
S-1	0.092	0.36	0.9945	0.348	0.40	0.9606	0.084	0.29	0.9852	0.378	0.32	0.9429	0.079	0.094	0.9835	1.039	0.105	0.9348
S-2	0.138	0.40	0.9987	0.550	0.43	0.9723	0.096	0.30	0.9909	0.426	0.34	0.9580	0.082	0.092	0.9808	1.115	0.102	0.9288
S-3	0.148	0.47	0.9946	0.517	0.50	0.9598	0.117	0.31	0.9881	0.574	0.33	0.9455	0.106	0.087	0.9823	1.702	0.096	0.9291
S-4	0.152	0.44	0.9933	0.587	0.47	0.9540	0.120	0.31	0.9919	0.562	0.34	0.9543	0.113	0.081	0.9845	2.014	0.088	0.9345

adsorption sites is heterogeneous on adsorbent surface (35). In comparison to the Freundlich model, the Langmuir model describes the isotherm data noticeably better for each pollutant. For the removal of Cd(II), the maximum adsorption capacity (q_m) is in the order of S-4 (267.8 mg g^{-1}) > S-3 (236.3 mg g^{-1}) > S-2 (170.1 mg g^{-1}) > S-1 (139.6 mg g^{-1}). However, an opposite result is found for the removal of CR, and q_m is in the order of S-1 (399.4 mg g^{-1}) > S-2 (394.1 mg g^{-1}) > S-3 (390.3 mg g^{-1}) > S-4 (368.3 mg g^{-1}). For the removal of MB, the greatest q_m is obtained by S-1 with a value of 576.6 mg g^{-1}, and lowest q_m is obtained by S-3 with a value of 563.6 mg g^{-1}. The interaction between adsorbent and dye molecules generally contains van der Waals forces, hydrogen bond and electrostatic interaction (36). The significant difference in the adsorption capacities between anionic and cationic dyes means the electrostatic interaction might play an important role in the adsorption.

3.2.3 Effect of pH

Since pH is one of the most important factors that may affect the adsorption capacity of adsorbent, the adsorption capacities of S-3 for Cd(II), MB and CR over a pH range of 2.0-6.0, 2.0-10.0 and 2.0-10.0, respectively, were investigated (Figure 7). For the removal of Cd(II), at lowest pH, the adsorption capacity is insignificant and it sharply increases with the increase of pH value. The change of pH value alters the surface charge on the hydrated Cd(II) ion, because pH affects the protonation or deprotonation of surface functional groups (37). pH also affects the charge of functional groups in polymer and Laponite. Increased H^+ ion restricts the approach of Cd(II) ion to the functional groups because of the repulsive force (38,39). For the removal of MB, an increase in solution pH apparently favors the adsorption capacity. This could also be due to the cationic characteristic of MB in aqueous solution. In contrast to Cd(II) and MB, CR removal seems to diminish with expanding the pH value. This may be attributed to the effect of acidic media on the surface of the adsorbent. The acidic conditions may cause surface protonation, and the adsorbent surface becomes positively charged (1).

3.2.4 Effect of temperature

Generally, two major effects on the adsorption process could be found from temperature. The temperature dependence of the adsorption system determines the adsorption to be endothermic or exothermic. Due to the decrease in viscosity of the solution, it is believed that increasing the temperature increases the rate of diffusion of the adsorbate. For the removal of Cd(II), there is an

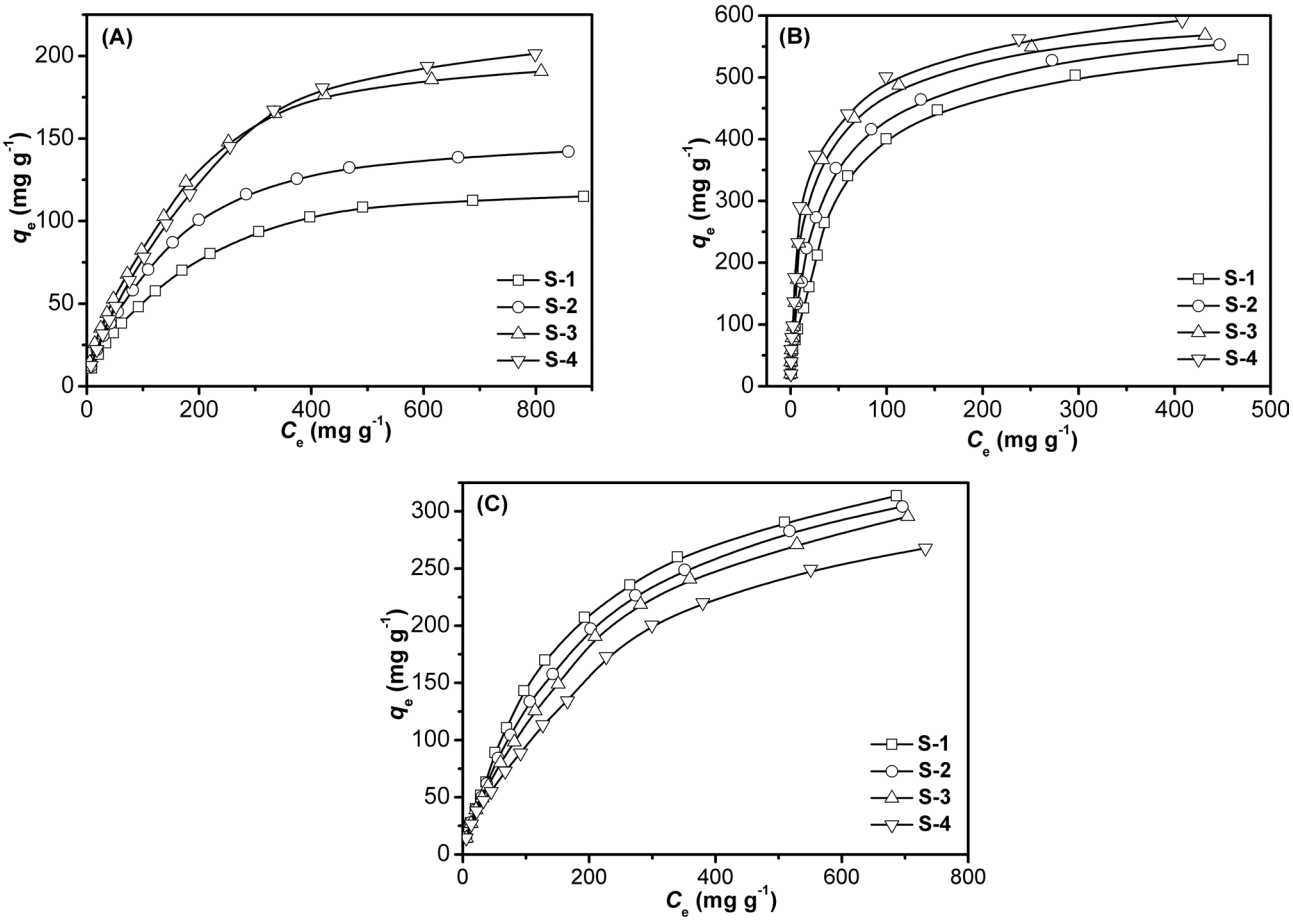

Figure 6: Adsorption isotherm on the adsorption of (a) Cd(II), (b) MB and (c) CR. (Conditions: time 90 min; pH 6.0; 30°C; adsorbent dosage 1 g L^{-1}).

obvious increase with temperature increasing from 20°C to 40°C, and a noticeable decrease with temperature increasing from 40°C to 60°C (Figure 8). The increase of temperature could facilitate the transfer of Cd(II) from aqueous solution into adsorbent, however, higher temperature may also induce the desorption process of pollutant, especially for the pollutant adsorbed by multilayer adsorption (40). For the removal of MB, the adsorption capacity increases from 426.5 mg g^{-1} to 509.1 mg g^{-1} when the temperature increases from 20°C to 60°C, and a continuous increase in the adsorption capacity can also be found for the adsorption of CR.

3.2.5 Effect of salt

Because almost all wastewater contains a certain amount of salt, the effect of salt (NaCl and $CaCl_2$) on the adsorption capacities of Cd(II), MB and CR onto S-3 was studied, and the results are shown in Figure 9. For the removal of Cd(II), a continuous decrease of adsorption capacity is observed in each salt solution, which could be attributed to the competitive binding of the cations for the surface functional groups of the adsorbent (41). When the concentration is 0.5 mol L^{-1}, the adsorption capacity is 133.2 mg g^{-1} and 124.8 mg g^{-1} for NaCl and $CaCl_2$, respectively. Compared to the monovalent cation, the divalent cation presents a more significant suppressive effect on Cd(II) adsorption, likely due to the stronger complexing ability of functional groups with Ca^{2+} ion (27). For the removal of MB, it is obvious that two salts play negative role on the performance. When the salt concentration increases from 0 to 0.5 mol L^{-1}, the adsorption capacity decreases from 433.7 mg g^{-1} to 377.2 and 355.6 mg g^{-1} for NaCl and $CaCl_2$, respectively. This negative effect might suggest that the ion-exchange interaction plays an important role during the adsorption process because the adsorbent is an anionic substance and MB is a cationic compound (42). With the increase of salt concentration, the active sites on the surface of the adsorbent and the active concentration of MB will decrease, causing the decrease of the interaction between positive charge and negative charge (43). For the removal of CR, the existence of salt is found to be favor for the adsorption property. The adsorption capacity in distilled water, NaCl solution (0.5 mol L^{-1}) and $CaCl_2$ solution

Table 4: Adsorption isotherm constants for Cd(II), MB and CR adsorbed by four adsorbents.

Sample	Cd(II)						MB						CR					
	Langmuir			Freundlich			Langmuir			Freundlich			Langmuir			Freundlich		
	q_m	K_L	R^2	K_F	n	R^2	q_m	K_L	R^2	K_F	n	R^2	q_m	K_L	R^2	K_F	n	R^2
S-1	139.6	0.0062	0.9951	7.48	2.38	0.9507	576.6	0.023	0.9912	65.67	2.79	0.9452	399.4	0.0057	0.9995	13.68	2.03	0.9642
S-2	170.1	0.0070	0.9964	9.86	2.42	0.9436	566.9	0.038	0.9910	83.60	3.05	0.9488	394.1	0.0049	0.9992	11.68	1.96	0.9738
S-3	236.3	0.0062	0.9932	11.28	2.27	0.9514	563.6	0.068	0.9862	110.09	3.44	0.9385	390.3	0.0043	0.9978	10.21	1.90	0.9766
S-4	267.8	0.0044	0.9950	8.04	2.00	0.9575	569.4	0.094	0.9840	121.31	3.53	0.9306	368.3	0.0038	0.9951	8.53	1.87	0.9784

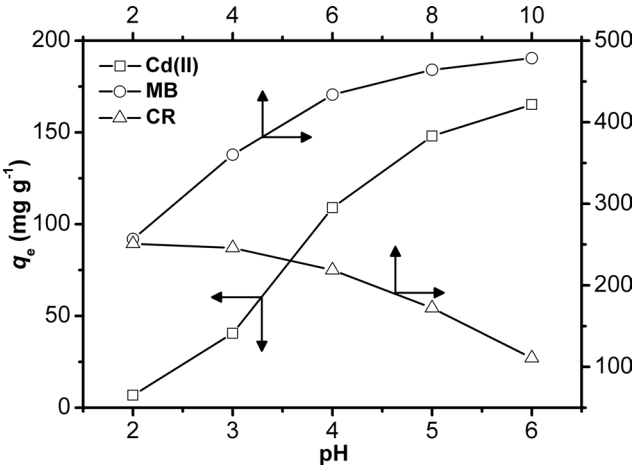

Figure 7: Effect of initial pH on the adsorption capacity of S-3. (Conditions: time 90 min; initial pollutant concentration 500 mg L^{-1}; 30°C; adsorbent dosage 1 g L^{-1}).

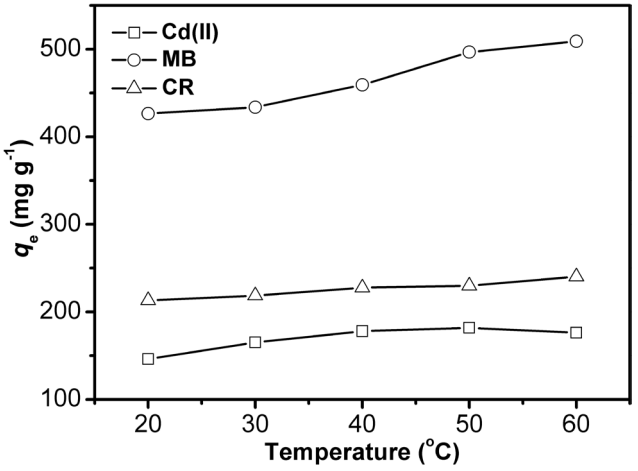

Figure 8: Effect of temperature on the adsorption capacity of S-3. (Conditions: time 90 min; initial pollutant concentration 500 mg L^{-1}; pH 6.0; adsorbent dosage 1 g L^{-1}).

(0.5 mol L^{-1}) is 218.7, 247.9 and 241.0 mg g^{-1}, respectively. The performance difference between MB and CR is mainly due to their different molecular structures. The introduction of salt may screen the electrostatic interaction between like charges, as a result, the electrostatic repulsion between the negative charged CR and the anionic adsorbent could be reduced (44,45).

3.3 Desorption studies

For practical point of view, reusability is an important feature of an advanced adsorbent because this reduces the material-cost significantly. According to our previous study, different solutions, such as HCl, EDTA, KCl and $CaCl_2$ solutions, were used as eluents for the regeneration

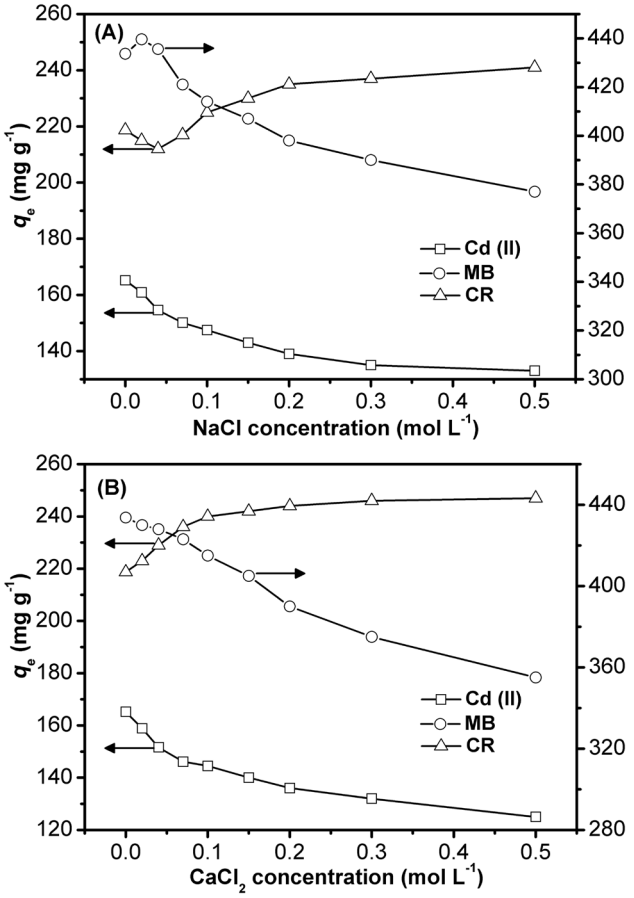

Figure 9: Effects of (a) NaCl and (b) $CaCl_2$ on the adsorption capacity of S-3. (Conditions: time 90 min; initial pollutant concentration 500 mg L^{-1}; pH 6.0; adsorbent dosage 1 g L^{-1}).

of this adsorbent after the adsorption of heavy metal ions, and dilute HCl solution was proved to be the most efficient one (3). During the removal process of Cd(II), the regeneration of S-3 with HCl solution (0.1 mol L^{-1}) was investigated as shown in Figure 10. After the first reuse cycle, a slight loss of adsorption capacity is observed, and the adsorption capacity remains broadly stable from the second reuse cycle to the fifth reuse cycle. After the fifth reuse cycle, the equilibrium adsorption capacity decreases from 165.2 mg g^{-1} to 151.8 mg g^{-1}. The dilute HCl or NaOH solution is not a proper eluent for the desorption of MB or CR Other methods, such as thermal desorption, and eluting with different kinds of organic solution (ethanol, methanol, acetic acid and a mixture of methanol and acetic acid) were tested, and the mixture of methanol and acetic acid (v/v, 9/1) was found to be the best eluent (46,47). After the fifth reuse cycle, the adsorption capacity decreases from 433.7 mg g^{-1} to 348.6 mg g^{-1}, and from 218.7 mg g^{-1} to 173.5 mg g^{-1} for the removal of MB and CR, respectively.

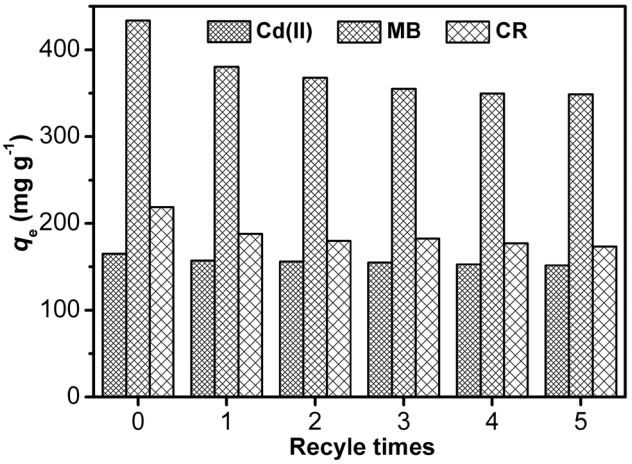

Figure 10: The regeneration and recycle of S-3.

3.4 Comparison of various adsorbents

The removal of heavy metal ions and dyes from aqueous solution has been extensively investigated by many adsorbents. Table 5 compares the adsorption capacities of the nanocomposite obtained in this work with different adsorbents previously used for the removal of pollutants. It can be seen that there are not many adsorbents capable of well adsorbing heavy metal ions, anionic dyes and cationic dyes simultaneously. Therefore, this nanocomposite adsorbent might be used as a universal adsorbent for different pollutants. In addition, the adsorption capacities of the nanocomposite adsorbent are much greater than that of many other previously reported adsorbents indicating that the as-prepared adsorbent has great potential application in pollutant removal from aqueous solution.

4 Conclusions

We successfully synthesized and characterized a chitosan and Laponite-based nanoparticle-polymer hybrid material. This nanocomposite adsorbent shows an excellent capacity for removing Cd(II), MB and CR from aqueous solution rapidly and efficiently due to its large surface area and total pore volume, which is enhanced by the Laponite component. With the increase of Laponite component in the adsorbent, the adsorption equilibrium time decreases from 35 min to 20 min. Additionally, this adsorbent exhibits a good reusability. In conclusion, this novel nanocomposite adsorbent is a promising material for wastewater treatment.

Table 5: Comparison of the maximum adsorption capacity of heavy metals, MB or CR onto different adsorbents.

Adsorbents	q_m (mg g^{-1})			References
	Heavy metals	MB	CR	
Laponite nanocomposite	236.3 (Cd)	563.6	390.3	This work
Serpentine	76.3 (Cr)	58.5	93.4	(1)
Katira gum based hydrogel	–	62.5	73.4	(10)
Polymer nanocomposite	158.8 (Ni)	–	–	(15)
Modified guar gum	–	–	226.2	(29)
Pyrolysis bio-char	–	16.9	–	(42)
Rice husk ash	–	18.1	7.0	(44)
Chelating resin	140.5 (Cd)	–	–	(48)
Activated carbon	–	934.6	–	(49)
Chitosan nanoparticle	12.2 (Cu)	–	–	(50)
Magnetic nanoparticle	56 (Cd)	–	–	(51)
Biogenic wastes	43.8 (Cd)	251.2	157.2	(52)

Acknowledgements: We appreciate the financial support from the National Natural Science Foundation of China (51874347, 21607174 and U1762212), the Fundamental Research Funds for the Central Universities (17CX02053), and the Program for Changjiang Scholars and Innovative Research Team in University (IRT_14R58).

References

1. Shaban M., Abukhadra M., Khan A., Jibali B., Removal of Congo red, methylene blue and Cr(VI) ions from water using natural serpentine. J Taiwan Inst Chem Eng, 2018, 82, 102-116.
2. Pérez-Marín A., Zapata V., Ortuño J., Aguilar M., Sáez J., Lloréns M., Removal of cadmium from aqueous solutions by adsorption onto orange waste. J Hazard Mater, 2007, 139(1), 122-131.
3. Cao J., Cao H., Zhu Y., Wang S., Qian D., Chen G., et al., Rapid and effective removal of Cu^{2+} from aqueous solution using novel chitosan and Laponite-based nanocomposite as adsorbent. Polymers, 2017, 9(1), 5.
4. Yin J., Blanch H., A bio-mimetic cadmium adsorbent: Design, synthesis, and characterization. Biotechnol Bioeng, 1989, 34(2), 180-188.
5. Boparai H., Joseph M., O'Carroll D., Kinetics and thermodynamics of cadmium ion removal by adsorption onto nano zerovalent iron particles. J Hazard Mater, 2011, 186(1), 458-465.
6. Benguella B., Benaissa H., Cadmium removal from aqueous solutions by chitin: Kinetic and equilibrium studies. Water Res, 2002, 36(10), 2463-2474.
7. Chowdhury S., Saha P., Adsorption kinetic modeling of safranin onto rice husk biomatrix using pseudo-first- and pseudo-second-order kinetic models: Comparison of linear and non-linear methods. Clean-Soil Air Water, 2011, 39(3), 274-282.
8. Gupta V., Ali I., Saini V., Removal of rhodamine B, fast green, and methylene blue from wastewater using red mud, an aluminum industry waste. Ind Eng Chem Res, 2004, 43(7), 1740-1747.
9. Vimonses V., Lei S., Jin B., Chow C., Saint C., Adsorption of congo red by three Australian kaolins. Appl Clay Sci, 2009, 43(3-4), 465-472.
10. Jana S., Ray J., Bhanja S., Tripathy T., Removal of textile dyes from single and ternary solutions using poly(acrylamide-*co*-*N*-methylacrylamide) grafted katira gum hydrogel. J Appl Polym Sci, 2018, 135(10), 45958.
11. Petrinic I., Korenak J., Povodnik D., Hélix-Nielsen C., A feasibility study of ultrafiltration/reverse osmosis (UF/RO)-based wastewater treatment and reuse in the metal finishing industry. J Clean Prod, 2015, 101, 292-300.
12. Korenak J., Ploder J., Trček J., Hélix-Nielsen C., Petrinic I., Decolourisations and biodegradations of model azo dye solutions using a sequence batch reactor, followed by ultrafiltration. Int J Environ Sci Technol, 2018, 15(3), 483-492.
13. Lau Y., Wong Y., Ang T., Ong S., Lutpi N., Ho L., Degradation reaction of Diazo reactive black 5 dye with copper (II) sulfate catalyst in thermolysis treatment. Environ Sci Pollut Res, 2018, 25(7), 7067-7075.
14. Anwar J., Shafique U., Salman M., Waheed-uz-Zaman, Anwar S., Anzano J., Removal of chromium (III) by using coal as adsorbent. J Hazard Mater,2009, 171(1-3), 797-801.
15. Rathika R., Byung-Taek O., Vishnukumar B., Shanthi K., Kamala-Kannan S., Janaki V., Synthesis, characterization and application of polypyrrole-cellulose nanocomposite for efficient Ni(II) removal from aqueous solution: Box-Behnken design optimization. e-Polymers, 2018, 18(4), 287-296.
16. Cao J., Tan Y., Che Y., Xin H., Novel complex gel beads composed of hydrolyzed polyacrylamide and chitosan: An effective adsorbent for the removal of heavy metal from aqueous solution. Bioresour Technol, 2010, 101(7), 2558-2561.

17. Xiong C., Pi L., Chen X., Yang L., Ma C., Zheng X., Adsorption behavior of Hg^{2+} in aqueous solutions on a novel chelating cross-linked chitosan microsphere. Carbohydr Polym, 2013, 98(1), 1222-1228.
18. Mittal H., Maity A., Ray S., The adsorption of Pb^{2+} and Cu^{2+} onto gum ghatti-grafted poly(acrylamide-co-acrylonitrile) biodegradablehydrogel: Isotherms and kinetic models. J Phys Chem B, 2015, 119(5), 2026-2039.
19. Awual M., Kobayashi T., Miyazaki Y., Motokawa R., Shiwaku H., Suzuki S., et al., Selective lanthanide sorption and mechanism using novel hybrid Lewis base (*N*-methyl-*N*-phenyl-1,10-phenanthroline-2-carboxamide) ligand modified adsorbent. J Hazard Mater, 2013, 252-253, 313-320.
20. Gotovac S., Yang C., Hattori Y., Takahashi K., Kanoh H., Kaneko K., Adsorption of polyaromatic hydrocarbons on single wall carbon nanotubes of different functionalities and diameters. J Colloid Interface Sci, 2007, 314(1), 18-24.
21. Vinu A., Murugesan V., Tangermann O., Hartmann M., Adsorption of cytochrome c on mesoporous molecular sieves: Influence of pH, pore diameter, and aluminum incorporation. Chem Mater, 2004, 16(16), 3056-3065.
22. Pinto M., Gonçalves R., Santos R., Araújo E., Perotti G., Macedo R., et al., Mesoporous carbon derived from a biopolymer and a clay: Preparation, characterization and application for an organochlorine pesticide adsorption. Microporous Mesoporous Mater, 2016, 225, 342-354.
23. Bandeira L., Calefi P., Ciuffi K., Faria E., Nassar E., Vicente M., et al., Preparation of composites of Laponite with alginate and alginic acid polysaccharides. Polym Int, 2012, 61(7), 1170-1176.
24. Chen P., Xu S., Wu R., Wang J., Gu R., Du J., A transparent Laponite polymer nanocomposite hydrogel synthesis via in-situ copolymerization of two ionic monomers. Appl Clay Sci, 2013, 72, 196-200.
25. Yang G., Tang L., Lei X., Zeng G., Cai Y., Wei X., et al., Cd(II) removal from aqueous solution by adsorption on α-ketoglutaric acid-modified magnetic chitosan. Appl Surf Sci, 2014, 292, 710-716.
26. Ngah W., Teong L., Hanafiah M., Adsorption of dyes and heavy metal ions by chitosan composites: A review. Carbohydr Polym, 2011, 83(4), 1446-1456.
27. Cao J., Fei D., Tian X., Zhu Y., Wang S., Zhang Y., et al., Novel modified microcrystalline cellulose-based porous material for fast and effective heavy-metal removal from aqueous solution. Cellulose, 2017, 24(12), 5565-5577.
28. Pálková H., Madejová J., Zimowska M., Serwicka E., Laponite-derived porous clay heterostructures: II. FTIR study of the structure evolution. Microporous Mesoporous Mater, 2010, 127(3), 237-244.
29. Pal S., Patra A., Ghorai S., Sarkar A., Mahato V., Sarkar S., et al., Efficient and rapid adsorption characteristics of templating modified guar gum and silica nanocomposite toward removal of toxic reactive blue and Congo red dyes. Bioresour Technol, 2015, 191, 291-299.
30. Cao J., Tan Y., Che Y., Ma Q., Fabrication and properties of superabsorbent complex gel beads composed of hydrolyzed polyacrylamide and chitosan. J Appl Polym Sci, 2010, 116(6), 3338-3345.
31. Leung W., Axelson D., Dyke J., Thermal degradation of polyacrylamide and poly(acrylamide-*co*-acrylate). J Polym Sci Pol Chem, 1987, 25(7), 1825-1846.
32. Singha N., Mahapatra M., Karmakar M., Dutta A., Mondal H., Chattopadhyay P., Synthesis of guar gum-*g*-(acrylic acid-coacrylamide-*co*-3-acrylamido propanoic acid) IPN *via in situ* attachment of acrylamido propanoic acid for analyzing superadsorption mechanism of Pb(II)/Cd(II)/Cu(II)/MB/MV. Polym Chem, 2017, 8(44), 6750-6777.
33. Huang Q., Liu M. Zhao J., Chen J., Zeng G., Huang H., et al., Facile preparation of polyethylenimine-tannins coated SiO_2 hybrid materials for Cu^{2+} removal. Appl Surf Sci, 2018, 427, 535-544.
34. Shen H., Zhu G., Yu W., Wu H., Ji H., Shi H., et al., Fast adsorption of *p*-nitrophenol from aqueous solution using *β*-cyclodextrin grafted silica gel. Appl Surf Sci, 2015, 356, 1155-1167.
35. Wei W., Wang Q., Li A., Yang J., Ma F., Pi S., et al., Biosorption of Pb (II) from aqueous solution by extracellular polymeric substances extracted from *Klebsiella* sp. J1: Adsorption behavior and mechanism assessment. Sci Rep, 2016, 6, 31575.
36. Li D., Li Q., Bai N., Dong H., Mao D., One-step synthesis of cationic hydrogel for efficient dye adsorption and its second use for emulsified oil separation. ACS Sustain Chem Eng, 2017, 5(6), 5598-5607.
37. Vahedi A., Rahmani M., Rahmani Z., Moghaddasi M., Rowshan F., Kazemi A., et al., Application of polymer-sepiolite composites for adsorption of Cu(II) and Ni(II) from aqueous solution: equilibrium and kinetic studies. e-Polymers, 2018, 18(3), 217-228.
38. Kalantari K., Ahmad M., Masoumi H., Shameli K., Basri M., Khandanlou R., Rapid and high capacity adsorption of heavy metals by Fe_3O_4/montmorillonite nanocomposite using response surface methodology: Preparation, characterization, optimization, equilibrium isotherms, and adsorption kinetics study. J Taiwan Inst Chem Eng, 2015, 49, 192-198.
39. Tseng J., Chang C., Chen Y., Chang C., Chiang P., Synthesis of micro-size magnetic polymer adsorbent and its application for the removal of Cu(II) ion. Colloids Surf A Physicochem Eng Asp, 2007, 295(1-3), 209-216.
40. Phetphaisit C., Yuanyang S., Chaiyasith W., Polyacrylamido-2-methyl-1-propane sulfonic acid-grafted-natural rubber as bio-adsorbent for heavy metal removal from aqueous standard solution and industrial wastewater. J Hazard Mater, 2016, 301, 163-171.
41. Wang J., Zheng S., Shao Y., Liu J., Xu Z., Zhu D., Amino-functionalized Fe_3O_4@SiO_2 core-shell magnetic nanomaterial as a novel adsorbent for aqueous heavy metals removal. J Colloid Interface Sci, 2010, 349(1), 293-299.

42. Liu Y., Zhao X., Li J., Ma D., Han R., Characterization of bio-char from pyrolysis of wheat straw and its evaluation on methylene blue adsorption. Desalin. Water Treat, 2012, 46(1-3), 115-123.
43. Guo J., Li B., Liu L., Lv K., Removal of methylene blue from aqueous solutions by chemically modified bamboo. Chemosphere, 2014, 111, 225-231.
44. Chowdhury A., Sarkar A., Bandyopadhyay A., Rice husk ash as a low cost adsorbent for the removal of methylene blue and Congo red in aqueous phases. Clean-Soil Air Water, 2009, 37(7), 581-591.
45. Zhu H., Zhang M., Liu Y., Zhang L., Han R., Study of Congo red adsorption onto chitosan coated magnetic iron oxide in batch mode. Desalin Water Treat, 2012, 37(1-3), 46-54.
46. Zhang X., Zhang P., Wu Z., Zhang L., Zeng G., Zhou C., Adsorption of methylene blue onto humic acid-coated Fe_3O_4 nanoparticles. Colloids Surf A Physicochem Eng Asp, 2013, 435, 85-90.
47. Mak S., Chen D., Fast adsorption of methylene blue on polyacrylic acid-bound iron oxide magnetic nanoparticles. Dyes Pigment, 2004, 16(1), 93-98.
48. Jiang J., Ma X., Xu L., Wang L., Liu G., Xu Q., et al., Applications of chelating resin for heavy metal removal from wastewater. e-Polymers, 2005, 15(3), 161-167.
49. Gong R., Ye J., Dai W., Yan X., Hu J., Hu X., et al., Adsorptive removal of methyl orange and methylene blue from aqueous solution with finger-citron-residue- based activated carbon. Ind Eng Chem Res, 2013, 52(39), 14297-14303.
50. Rahmani O., Bouzid B., Guibadj A., Extraction and characterization of chitin and chitosan: Applications of chitosan nanoparticles in the adsorption of copper in an aqueous environment. e-Polymers, 2017, 17(5), 383-397.
51. Chen D., Awut T., Liu B., Ma Y., Wang T., Nurulla I., Functionalized magnetic Fe_3O_4 nanoparticles for removal of heavy metal ions from aqueous solutions. e-Polymers, 2016, 16(4), 313-322.
52. Babalola J., Olowoyo J., Durojaiye A., Olatunde A., Unuabonah E., Omorogie M., Understanding the removal and regeneration potentials of biogenic wastes for toxic metals and organic dyes. J Taiwan Inst Chem Eng, 2016, 58, 490-499.